



# LUND UNIVERSITY

## Low-band MIMO antenna for smartphones with robust performance to user interaction

Aliakbari Abar, Hanieh; Lau, Buon Kiong

*Published in:*  
IEEE Antennas and Wireless Propagation Letters

*DOI:*  
[10.1109/LAWP.2021.3075240](https://doi.org/10.1109/LAWP.2021.3075240)

2021

*Document Version:*  
Peer reviewed version (aka post-print)

[Link to publication](#)

*Citation for published version (APA):*  
Aliakbari Abar, H., & Lau, B. K. (2021). Low-band MIMO antenna for smartphones with robust performance to user interaction. *IEEE Antennas and Wireless Propagation Letters*, 20(7), 1195 - 1199.  
<https://doi.org/10.1109/LAWP.2021.3075240>

*Total number of authors:*  
2

### General rights

Unless other specific re-use rights are stated the following general rights apply:  
Copyright and moral rights for the publications made accessible in the public portal are retained by the authors and/or other copyright owners and it is a condition of accessing publications that users recognise and abide by the legal requirements associated with these rights.

- Users may download and print one copy of any publication from the public portal for the purpose of private study or research.
- You may not further distribute the material or use it for any profit-making activity or commercial gain
- You may freely distribute the URL identifying the publication in the public portal

Read more about Creative commons licenses: <https://creativecommons.org/licenses/>

### Take down policy

If you believe that this document breaches copyright please contact us providing details, and we will remove access to the work immediately and investigate your claim.

LUND UNIVERSITY

PO Box 117  
221 00 Lund  
+46 46-222 00 00

# Low-Band MIMO Antenna for Smartphones with Robust Performance to User Interaction

Hanieh Aliakbari, *Graduate Student Member, IEEE*, and Buon Kiong Lau, *Senior Member, IEEE*

**Abstract**—This letter proposes a two-port MIMO smartphone antenna for frequency bands below 1 GHz, which is robust to user effects. The design is achieved by first analyzing the characteristic modes of a chassis that includes the large screen. Two modes predicted to be less affected by the user than other commonly used modes are selected. The modal currents and near-fields of the two desired modes then guide the design: The monopole-like mode introduced by the screen is tuned to resonance using shorting pins and selectively excited using the center feed location. The non-resonant loop mode is selectively excited for the first time by four inductive feeds added along the longer sides of the chassis, with proper phase shifts provided by a feeding network. The proposed antenna features isolation of above 19 dB and envelope correlation coefficient of below 0.12 in the considered scenarios. The measured bandwidth is above 15% for both ports, and the average radiation efficiency is 2 dB and 4.57 dB higher for two user scenarios with respect to a reference design. Moreover, no adaptive matching is needed as the impedance matching is robust to the user hand/head.

**Index Terms**—Handset antennas, MIMO systems, user effect, characteristic modes, feeding network.

## I. INTRODUCTION

MULTIPLE-input multiple-output (MIMO) antenna design for smartphones is very challenging, especially in frequency bands below 1 GHz (i.e., LTE low band), since sufficiently large bandwidth and low correlation are required for an electrically compact chassis [1]. Fortunately, characteristic mode analysis (CMA) can be used to design uncorrelated MIMO antennas of up to 30% bandwidths by using the chassis' modal properties to tune several modes and excite them [1]–[4].

Another challenging issue is that smartphone antennas are traditionally designed and characterized for free space (FS) operation, rather than actual use cases that involve the close proximity of user hands and head [5]. The high permittivity and high conductivity of the human tissue can result in severe detuning of the antenna and significant power absorption, respectively, which deteriorate antenna efficiency [6]. For instance, the effect of user hand on the operation of a single port antenna is presented in [7], indicating a 7–11 dB drop in antenna efficiency in a LTE low band, compared to FS. In a few studies on the performance of MIMO handsets in the low band [8]–[11], the proximity of the human body is shown to severely affect both efficiency and correlation of two-port MIMO antennas. Depending on the position of the index finger, the variation in mutual coupling of two-port MIMO antennas can be up to 10 dB [8]. In [9], the far-field patterns of a MIMO antenna is found

to be more correlated when the head is in proximity. Another investigation in [10] found that the total efficiency can be as low as -19.1 dB, due to the absorption and mismatch by the user's hand and head, compared to -1.9 dB in FS. In [11], a user hand causes a 4 dB loss in the average total efficiency of a highly correlated MIMO antenna at 0.75 GHz.

Due to the aforementioned significant user effects on MIMO antenna performance, it is important to not only evaluate the performance of completed antenna prototypes in different user scenarios after the design stage [8]–[11], but to also account for user interactions at the design stage. For instance, some design techniques have been found to be effective for mitigating user effects in terminal antennas in LTE low band [12]–[23]. However, existing contributions focus on single-antenna design [12]–[20] and only a few consider MIMO antennas [21]–[23].

In [21], the least affected antenna of four identical elements located at four edges of the chassis is dynamically selected to overcome user effects. Using adaptive matching, significant capacity gains have been achieved in the presence of user by targeting low correlation [22]. However, these methods [21], [22] require complex adaptive circuits and the MIMO antennas utilize only the traditional fundamental dipole mode of the chassis, which is known to be vulnerable to user effects [19].

A comparison study in [23] reveals that the CMA-based MIMO terminal antennas are in general more robust to user effects in the low band, in terms of impedance matching and correlation. Moreover, it has been found that the excited modes of an antenna can substantially influence its user effects [18]–[20]. Since the antenna pattern is a linear combination of the far-fields of the characteristic modes (CMs) excited by the antenna, the user effects on a given CM can be found. In [19], it is observed that the characteristic far-field patterns with a null at the boresight are less affected by a user hand, by comparing the modal weighting coefficients of the antenna in FS with those in the hand grip. This result can be understood by the severe shadowing by the palm and fingers at the boresight. It is not uncommon in the literature to utilize far-field properties to guide antenna designs involving proximity of human tissue, due to the lack of consensus on a suitable near-field figure-of-merit [24]. Subsequently, this insight is applied using CMA to synthesize a desired antenna pattern consisting of several chassis modes [20]. However, the design is single-port and the achieved bandwidth is small (6%).

In this work, we extend this promising concept to design a robust two-port MIMO smartphone antenna in a systematic manner using CMA. The proposed design offers >15% bandwidth and <0.07 envelope correlation coefficient (ECC) in free space, in LTE low band. Since the screen-to-body ratio of smartphones is increasing nowadays [25]–[27], the two CMs

Manuscript received February 15, 2021; revised 1 April 2021; accepted 20 April 2021. This work was supported by Vetenskapsrådet (Dnr 2018-04717).

Hanieh Aliakbari and Buon Kiong Lau are with the Department of Electrical and Information Technology, Lund University, 221 00 Lund, Sweden (E-mails: {hanieh.aliakbari\_abar, buon\_kiong.lau}@eit.lth.se).

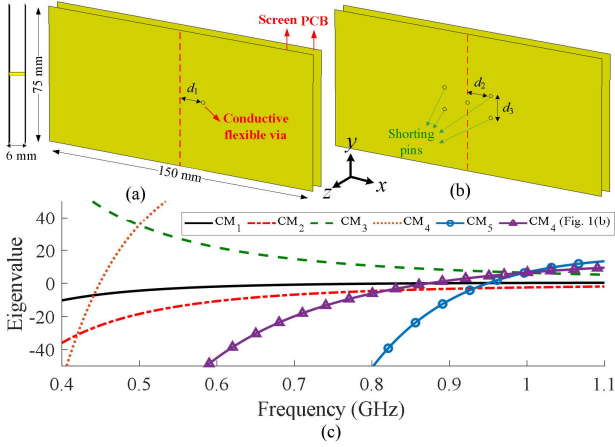


Fig. 1. (a) Geometry of the connected metal plates, (b) geometry with  $d_1 = 0$  mm and 4-metal pins added ( $d_2 = 9$  mm,  $d_3 = 5$  mm), and (c) Eigenvalues  $\lambda_n$  of the modes of interest for the dual-plate model in (a) and (b). Eigenvalues of CM1-CM3, CM5 are similar for (a) and (b).

utilized in the design are based on a chassis model that includes a large metal-backed screen. The two modes are selectively excited by the two ports, yielding the desired antenna patterns that have nulls at the boresight. Finally, the MIMO antenna is confirmed to be robust to two common user scenarios.

## II. CMA OF CONNECTED DOUBLE PLATE MODEL

Two connected parallel metal plates are used as a model for a large screen smartphone [28] (see Fig. 1(a)). As shown in the smartphone model, there is a conductive flexible via (represented by a conductive pin of 1 mm in diameter, located  $d_1$  above the center of each plate) that connects the screen assembly to the PCB [25]-[27]. In this section, CMA is performed using 2019 Altair FEKO to explore the modes of this connected perfect electric conductor (PEC) double-plate model.

For the initial analysis, the screen size is set to be the same as the PCB size (see Fig. 1(a)). We denote the first mode (CM1) as the longitudinal half-wave ( $0.5\lambda$ ) dipole mode, the second one (CM2) as the transversal  $0.5\lambda$ -dipole mode and the third one (CM3) as the loop mode (see Fig. 2(a)), all of which also exist in single-PCB models [1]. On the other hand, two new CMs (CM4, CM5) are found for the double-plate model in Fig. 1(a). The lowest-order mode (CM4) is a monopole-like mode that is due to two connected plates and the fifth mode (CM5) is a patch-like mode due to the added screen at the distance of  $h$  to the PCB (see Fig. 1(a)). According to the concept in [29], shorting pins can be introduced to shorten the current paths and hence increase the resonant frequency of the zeroth-order mode. Four shorting pins were introduced (see Fig. 1(b)) to increase the low resonant frequency (0.45 GHz) of CM4 to the desired low LTE band [27]. The eigenvalues of CM1-CM5 for the models in Figs. 1(a) and 1(b) with the four shorting pins are shown in Fig. 1(c). The corresponding far field patterns are presented in Fig. 2(a). It is noted that apart from CM4, the eigenvalues and far-fields of the four other modes are identical between the two models shown in Fig. 1. The reason is that the pins are located in the minimum near-field region of the four other modes (e.g. see Fig. 3(a) for that of CM5). Most of the existing terminal antennas in LTE low band use the longitudinal  $0.5\lambda$ -dipole mode (CM1) and/or the transversal  $0.5\lambda$ -dipole mode (CM2)

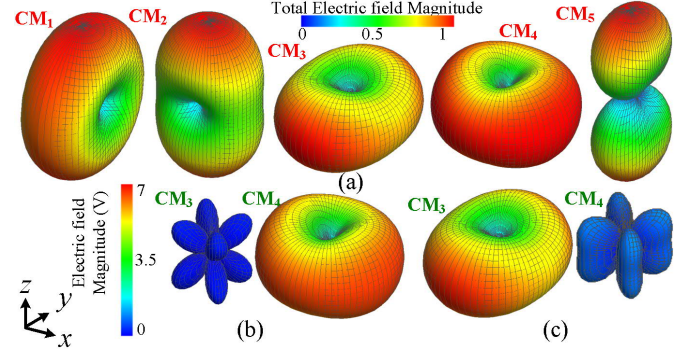


Fig. 2. (a) The normalized characteristic far-field patterns for CMs in Fig. 1(c), electric field magnitude of (b) theta and (c) phi components of CM3 and CM4.

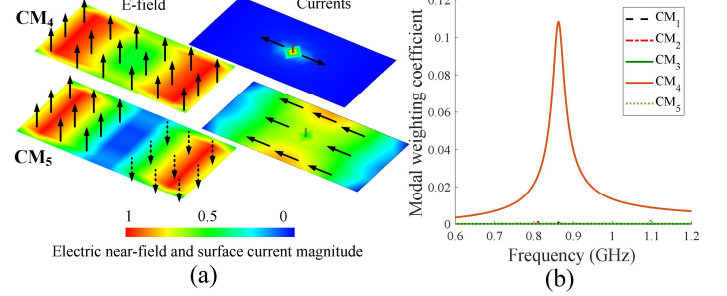


Fig. 3. (a)  $z$ -directed electric near-field in between two plates and modal current for CM4 and CM5, (b) modal weighting coefficient for the first port ( $P_1$ ).

[1]-[17], [21]-[27]. The patterns of these dipole modes are omnidirectional on the planes perpendicular to the PCB, i.e.,  $yz$ - and  $xz$ -planes (see Fig. 2(a)). Similarly, a patch-like mode (CM5) also has more directional patterns on the planes perpendicular to the PCB. If the terminal antenna utilizes these modes (CM1, CM2, CM5), then the antenna will illuminate the user in both near- and far-fields and suffers more from user effects [19].

To reduce the user effect, an omni-directional pattern with radiation nulls in the boresight direction, i.e., along the positive and negative of  $z$ -axis, is preferred [20]. As shown in Fig. 2(a), CM3 and CM4 are good candidates for this goal as they provide the desired omni-directional pattern on the  $xy$ -plane, with the nulls along the  $z$ -axis. Despite having similar gain patterns, CM3 and CM4 are orthogonal. This due to polarization diversity (see Figs. 2(b) and 2(c)), with the phi and theta components being dominant for CM3 and CM4, respectively. Consequently, they are good candidates for implementing two orthogonal ports with less effects from user. Therefore, in contrary to previously reported multiport terminal antennas in the low band, the excitation of commonly used modes of CM1, CM2 and CM5 are avoided in the proposed MIMO antenna (PMA).

## III. SELECTIVE EXCITATION OF CM4 BY PORT 1 ( $P_1$ )

As explained in Section II, CM4 is tuned to the desired band by adding several shorting pins. The next task is to excite this mode using  $P_1$ , and to prevent the same port from exciting other resonant modes. The characteristic electric field (E-field) distribution half-way between the two plates (i.e., 3 mm from either plate) and current distributions are shown for CM4 and CM5 in Fig. 3(a). The characteristic E-field of CM4 is almost consistently in the  $z$ -direction in the volume between the plates. The E-field for CM5 is in both positive (top half) and negative (bottom half)  $z$ -directions, with the minimum E-field occurring

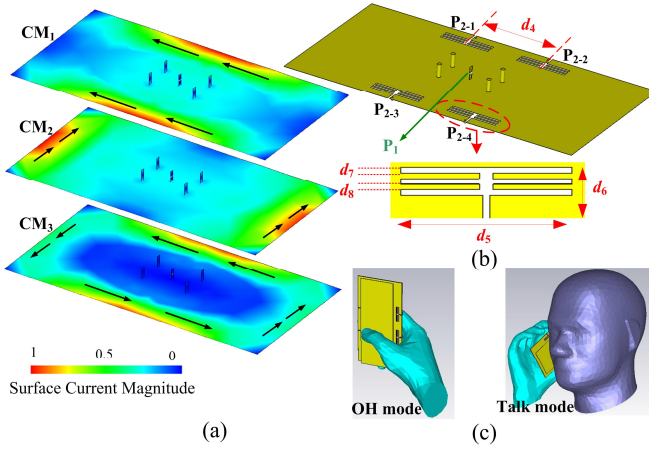


Fig. 4. (a) Surface current on PCB for CM<sub>1</sub>-CM<sub>3</sub>, (b) four added slots (ICE) with parameters on the PCB ( $d_4 = 40$  mm,  $d_5 = 23$  mm,  $d_6 = 10$  mm,  $d_7 = d_8 = 1$  mm). Screen is not shown for clarity, and (c) antenna in two user scenarios.

around the center. So the center feed (i.e., P<sub>1</sub> in Fig. 4(b)) can be used to prevent excitation of CM<sub>5</sub>. This is the reason initially for setting  $d_1 = 0$  in Fig. 1(b). Moreover, using this single feed should not excite CM<sub>1</sub>, CM<sub>2</sub> and CM<sub>3</sub>, as their currents are very small along the via between the plates, as shown in Fig. 4(a). This is different from the feeding consideration in [27], where the goal is to simultaneously excite CM<sub>4</sub> and CM<sub>5</sub>. In contrast, the goal here is to selectively excite CM<sub>4</sub>, to provide the desired omni-directional pattern on the  $xy$ -plane for P<sub>1</sub> in the low band, with the nulls along the  $z$ -axis.

The shorting pins are located around the feed in the center as shown in Fig. 1(b), instead of being placed in a single row [27]. The more symmetrical structure helps to prevent the excitation of undesired modes in the final design. The selective excitation of CM<sub>4</sub> was verified by using the modal weighting coefficients for P<sub>1</sub>, shown in Fig. 3(b). The selective excitation strategy allows another CM with radiation nulls in the boresight (i.e., CM<sub>3</sub>) to be used for the other port, and low correlation with the other port is guaranteed as long as that port does not excite CM<sub>4</sub>.

#### IV. SELECTIVE EXCITATION OF CM<sub>3</sub> BY PORT 2 (P<sub>2</sub>)

CM<sub>3</sub> is a loop mode which also exists for a single chassis. CM<sub>3</sub> has long been recognized as an inherently non-resonant inductive mode [1], hence it has not been considered practical for antenna design. To our knowledge, this work represents the first time this mode is successfully utilized for MIMO terminal antenna design. The surface current distribution of CM<sub>1</sub>-CM<sub>3</sub> on the PCB is shown in Fig. 4(a). The directions of the surface currents on the screen (not shown in Fig. 4(a)) are the same as those on the PCB for CM<sub>1</sub>-CM<sub>3</sub>, and the current is minimum on the conductive flexible via. To excite the loop-like surface currents of CM<sub>3</sub> on the PCB, four small inductive coupling elements (ICEs) are implemented symmetrically along the longer sides of the PCB, as depicted in Fig. 4(b). Four voltage ports (i.e., P<sub>2-1</sub>-P<sub>2-4</sub> in Fig. 4(b)) are directly positioned across each of the ICEs. By this arrangement, the two shorter sides of the chassis can be used by other antenna elements to cover other bands. The configuration of the ICE in Fig. 4(b) is the cascaded version of that in [30], which is used to ease the matching of CM<sub>3</sub> across the band. The ICEs have no noticeable effect on the eigenvalues (Fig. 1(c)) and far-fields (Fig. 2(a)) of the CMs. To

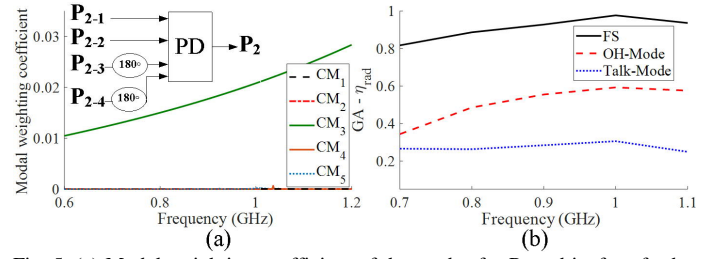


Fig. 5. (a) Modal weighting coefficient of the modes for P<sub>2</sub> and its four feeds with phase shift. A power divider (PD) is used. (b) GA- $\eta_{\text{rad}}$  for three scenarios.

excite the desired modes, the correct relative amplitudes and phase shifts corresponding to the modal currents in Fig. 4(a) should be applied to P<sub>2-1</sub>-P<sub>2-4</sub>. Accordingly, P<sub>2-1</sub> and P<sub>2-2</sub> should be phase shifted by 180° relative to P<sub>2-3</sub> and P<sub>2-4</sub>, as seen in the inset of Fig. 5(a). The modal weighting coefficients (see Figs. 5(a)) confirm the correct selective feeding of CM<sub>3</sub>. If no phase shift is applied, then the ICEs will excite CM<sub>1</sub> and CM<sub>5</sub> instead, due to their in-phase currents at these feed positions.

To explain how CM<sub>3</sub> can be used by port 2 despite being non-resonant, it can be seen in Fig. 1(c) that the eigenvalue of the CM<sub>3</sub> at 0.9 GHz is about 8.68. However, due to the use of more coupling elements the modal excitation coefficient of CM<sub>3</sub> can be increased accordingly [31]. Therefore, efficient excitation of CM<sub>3</sub> by the feeds that are well-aligned to the modal properties has partly compensated for the relatively large eigenvalue of CM<sub>3</sub>. Consequently, this work offers the new insight that additionally flexibility can be gained for antenna design using CMA by considering the feeding structure. Specifically, the possible use of a given CM not only depends on the magnitude of its eigenvalues, but also on how the feed can be designed to enhance the excitation of a CM to compensate for relatively large eigenvalues. This insight will allow more CMs to be chosen as candidate modes for antenna design.

#### V. USER EFFECT AND SIMULATED RESULTS

The robustness of the proposed two-port design is evaluated in free space (FS) and two user scenarios (one-hand (OH) browse mode and talk mode [23], see Fig. 4(c)) using the time-domain solver of CST 2018. The radiation efficiencies of P<sub>1</sub> and P<sub>2</sub> are 94% and 91% in FS at 0.9 GHz, and they drop to 60% and 52%, respectively, in OH. The radiation efficiencies of the proposed design are less affected than the design with broadside pattern in [15] (1.94/2.4 dB drop for P<sub>1</sub>/P<sub>2</sub> vs. 4 dB in [15]). The geometric average of radiation efficiencies (GA- $\eta_{\text{rad}}$ ) over the two ports as defined in [23] is shown in Fig. 5(b) for the PMA. Since [15] only considers a single-port antenna and a OH mode, better benchmarking can be obtained using the CMA-based two-port antenna evaluated in [23] (see Fig. 6(a)) as a reference MIMO antenna (RMA). The RMA uses modes with no null in the broadside for both ports (i.e., port 1 excites full-wave loop mode and port 2 excites the fundamental dipole mode). To ensure fair comparison, the positions of the coupling element and feeding lines in the chosen RMA are similar to those of the PMA. As can be seen in Fig. 6(b), the drop in the radiation efficiencies of the RMA are 2 dB and 4.57 dB higher than those of the PMA, in the OH mode and talk mode, respectively. Moreover, the matching efficiency [23] of the RMA is reduced more than that of the PMA in the two user scenarios (see Fig.



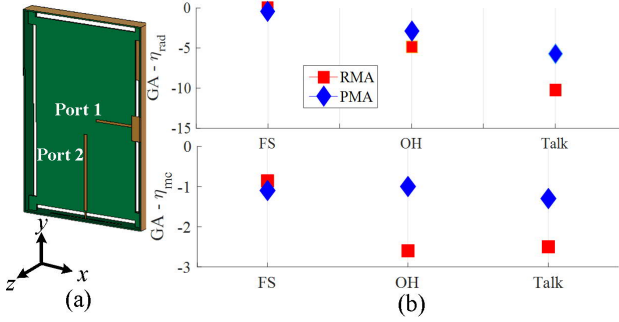


Fig. 6. (a) RMA (i.e. prototype 1 in [23]), (b) comparison of  $GA-\eta_{rad}$  and  $GA-\eta_{mc}$  over operating bands in three scenarios for RMA and PMA.

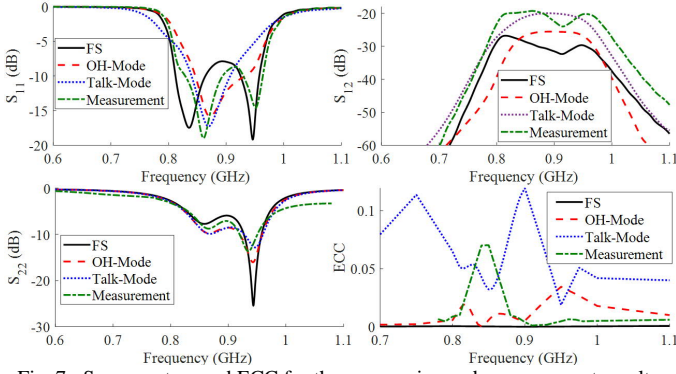


Fig. 7. S-parameters and ECC for three scenarios and measurement results.

6(b)) over 836-968 MHz. Figures 6(b) and 7 show that the S-parameters for the PMA is more stable with acceptable matching and isolation in different scenarios, indicating its robustness to user effects. The ECC is below 0.12 in all the scenarios (see Fig. 7). The slightly higher ECC in the talk mode is mainly due to the shadowing of the patterns by the user, which increases the similarity between the two patterns. It is noted that the comparison of  $\eta_{rad}$  of the individual ports also shows better performance for the PMA ports. Comparisons with other two-port antennas are also provided in Table I.

## VI. MEASURED RESULTS

In real implementation, microstrip lines are used to feed the ICEs instead of direct voltage ports (see Fig. 8). The ICEs are etched on the top side of the chassis, with matching elements placed on the substrate. The feeding network realized by microstrip lines is printed on the back side of the chassis. The matching elements shown in Fig. 8 are used to widen the bandwidth. The substrate used is Rogers RO4003C (thickness of 1.524 mm, relative permittivity of 3.38 and loss tangent of 0.0027). Three PDs with different phase shifts (PSs) are used in Fig. 8 to feed the ICEs. As all the ICEs are similar and distributed in a mirror symmetric manner, there is ideally no power dissipation in the PDs. The advantage of using PDs over T-divider, despite the earlier being more space consuming, is that the matching is more controllable due to the isolation between the PDs' ports [33], [34]. It is noted that the simple feeding networks in Fig. 8 are only intended to verify the operation of the PMA. In real implementation, the PD, PS and off-chip matching elements should be realized with compact integrated circuits for the sake of practicality and compactness, and optimized with respect to the active RF circuitry. The feeding network in Fig. 8 can be realized in any advanced multilayer technology [35].

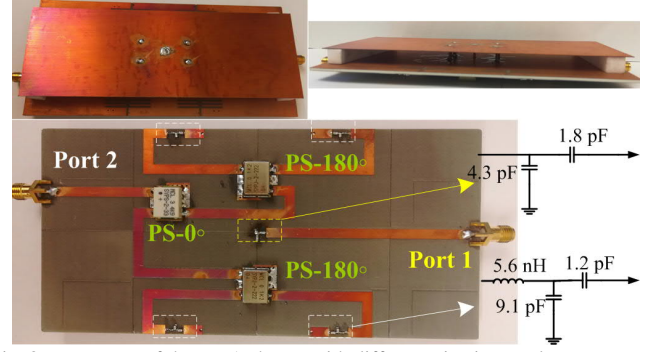


Fig. 8. Prototype of the PMA shown with different viewing angles.

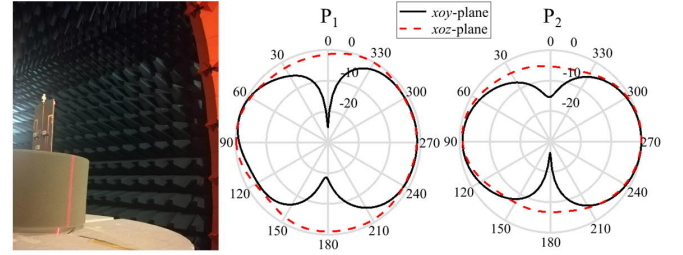


Fig. 9. Measured radiation patterns in two planes for two ports.

COMPARISON OF THE PMA AND TWO-PORT ANTENNAS IN LOW BAND					
Ref.	Common BW(MHz)	Ave. $GA-\eta_{tot}$ (OH)	Ave. $GA-\eta_{tot}$ (Talk)	Ave. ECC (OH/Talk)	Adaptive network
[21]*	750–960	-6.88 dB	-10.57 dB	0.13/0.17	Yes
[22]	815–875	-5.5 dB	N/A	0.03/NA	Yes
[23]**	824–894	-7.5 dB	-12.77 dB	0.03/0.15	No
[23]***	818–896	-4.5 dB	-14 dB	0.04/0.02	No
[32]	829–960	-6.59 dB	N/A	0.05/NA	No
[10]*	746–787	N/A	-14.6 dB*	NA/0.05	No
<b>PMA</b>	<b>836–968</b>	<b>-3.9 dB</b>	<b>-7 dB</b>	<b>0.02/0.06</b>	<b>No</b>

\* Best prototypes (i.e. Antenna34 in [21], and P<sub>2</sub> in [10]), \*\* Prototype 1 (i.e., RMA), and \*\*\* Prototype 2 in [23]

For the final layout in Fig. 8, the size of the screen is slightly decreased to increase the potential bandwidth [36] of CM<sub>3</sub>. The measured bandwidths are 18% (805-967 MHz) and 15% (836-968 MHz) for P<sub>1</sub> and P<sub>2</sub>, respectively, which agree well with the simulation results (see Fig. 7). The measured isolation is over 19 dB. The average in-band total efficiencies are 81% and 68% (minimum of 65% and 63%) for P<sub>1</sub> and P<sub>2</sub>, respectively. The lower total efficiency in P<sub>2</sub> is mainly due to the PD's loss in the feeding network of Fig. 8. The measured radiation patterns of the two ports (see Fig. 9) show that the radiation nulls are successfully retained at the boresight and backward directions as for CM<sub>3</sub> and CM<sub>4</sub> in Fig. 2. Finally, the ECC of the measured patterns (see Fig. 7) is below 0.07 in the operating band.

## VII. CONCLUSION

Using the connected metal-backed screen and chassis model, two new modes are selected and excited for the first time using CMA, resulting in a two-port MIMO terminal antenna for LTE low band. The two ports are more robust in two user scenarios than a reference design, due to the selected modes having a desirable property. Therefore, the proposed antenna does not require any adaptive circuit to compensate for user effects.

## ACKNOWLEDGMENT

The authors would like to thank Andreas Johansson of Lund University and Dymtro Pugachev of Sigma Connectivity AB for their help in prototype fabrication and pattern measurement.

## REFERENCES

- [1] H. Li, Z. Miers, and B. K. Lau, "Design of orthogonal MIMO handset antennas based on characteristic mode manipulation at frequency bands below 1 GHz," *IEEE Trans. Antennas Propag.*, vol. 62, no. 5, pp. 2756–2766, May 2014.
- [2] S. Zhang, K. Zhao, Z. Ying, and S. He, "Investigation of diagonal antenna-chassis mode in mobile terminal LTE MIMO antennas for bandwidth enhancement," *IEEE Antennas Propag. Mag.*, vol. 57, no. 2, pp. 217–228, Apr. 2015.
- [3] C. Deng, Z. Feng, and S. V. Hum, "MIMO mobile handset antenna merging characteristic modes for increased bandwidth," *IEEE Trans. Antennas Propag.*, vol. 64, no. 7, pp. 2660–2667, Jul. 2016.
- [4] H. Aliakbari, and B. K. Lau, "Low-profile two-port MIMO terminal antenna for low LTE bands with wideband multimodal excitation," *IEEE Open J. Antennas Propag.*, vol. 1, pp. 368–378, 2020.
- [5] R. Khan, A. Al-Hadi, and P. J. Soh, "Recent advancements in user effect mitigation for mobile terminal antennas: A review," *IEEE Trans. Electromagn. Compat.*, vol. 61, no. 1, pp. 279–287, Feb. 2019.
- [6] B. K. Lau, "Multiple antenna terminals," in *MIMO: From Theory to Implementation*. New York, NY, USA: Academic, 2010, pp. 267–298.
- [7] J. Holopainen, O. Kiveks, J. Ilvonen, R. Valkonen, C. Icheln, and P. Vainikainen, "Effect of the user's hands on the operation of lower UHF band mobile terminal antennas: Focus on digital television receiver," *IEEE Trans. Electromagn. Compat.*, vol. 53, no. 3, pp. 831–841, Aug. 2011.
- [8] A. A.-H. Azremi, J. Ilvonen, C.-H. Li, J. Holopainen, and P. Vainikainen, "Influence of the user's hand on mutual coupling of dual-antenna structures on mobile terminal," in *Proc. 6th Eur. Conf. Antennas Propag.*, Prague, Czech Republic, Mar. 26–30, 2012, pp. 1222–1226.
- [9] A. Hussain, P.-S. Kildal, U. Carlberg, and J. Carlsson, "Correlation between far-field patterns on both sides of the head of two-port antenna on mobile terminal," in *Proc. Int. Symp. Antennas Propag.*, vol. 1, Nanjing, China, Oct. 23–25, 2013, pp. 288–289.
- [10] E. Buskgaard, A. Tatomirescu, S. C. Del Barrio, O. Franek, and G. F. Pedersen, "User effect on the MIMO performance of a dual antenna LTE handset," in *Proc. 8th Eur. Conf. Antennas Propag.*, The Hague, Netherlands, Apr. 6–11, 2014, pp. 2006–2009.
- [11] R. Tian, B. K. Lau, and Z. Ying, "Multiplexing efficiency of MIMO antennas with user effects," in *Proc. IEEE Int. Symp. Antennas Propag.*, Chicago, IL, Jul. 8–14, 2012, pp. 1–2.
- [12] R. Valkonen, J. Ilvonen, K. Rasilainen, J. Holopainen, C. Icheln, and P. Vainikainen, "Avoiding the interaction between hand and capacitive coupling element based mobile terminal antenna," in *Proc. 5th Eur. Conf. Antennas Propag.*, Rome, Italy, Apr. 11–15, 2011, pp. 2781–2785.
- [13] M. Berg, M. Sonkki, and E. T. Salonen, "Absorption loss reduction in a mobile terminal with switchable monopole antennas," *IEEE Trans. Antennas Propag.*, vol. 59, no. 11, pp. 4379–4383, Nov. 2011.
- [14] J. Ilvonen, R. Valkonen, O. Kiveks, P. Li, and P. Vainikainen, "Antenna shielding method reducing interaction between user and mobile terminal antenna," *Electron. Lett.*, vol. 47, no. 16, pp. 896–897, 2011.
- [15] J. Lee, J. Lee, K. Min, and Y. Cheon, "Miniaturized antennas with reduced hand effects in mobile phones using magneto-dielectric material," *IEEE Antennas Wireless Propag. Lett.*, vol. 13, pp. 935–938, 2014.
- [16] A. Andujar, J. Anguera, Y. Cobo, and C. Picher, "Distributed antenna systems for wireless handheld devices robust to hand loading," *IEEE Trans. Antennas Propag.*, vol. 60, no. 10, pp. 4830–4837, Oct. 2012.
- [17] M. R. Islam and M. Ali, "Ground current modification of mobile terminal antennas and its effects," *IEEE Antennas Wireless Propag. Lett.*, vol. 10, pp. 438–441, 2011.
- [18] S. J. Kim, *et al.*, "Ground plane with loop structure for reducing user's hand effect," *IEEE Antennas Wireless Propag. Lett.*, vol. 11, pp. 450–452, Apr. 2012.
- [19] M. Wu, B. Wang, H. Li, and Y. Yu, "Reducing user effects on mobile handset antennas using mode mapping," in *Proc. 14th Eur. Conf. Antennas Propag.*, Copenhagen, Denmark, Mar. 15–20, 2020.
- [20] H. Li, S. Sun, W. Li, M. Wu, and C. Zhou, "Systematic pattern synthesis for single antennas using characteristic mode analysis," *IEEE Trans. Antennas Propag.*, vol. 68, no. 7, pp. 5199–5208, Mar. 2020.
- [21] S. Zhang, K. Zhao, Z. Ying, and S. He, "Adaptive quad-element multi-wideband antenna array for user-effective LTE MIMO mobile terminals," *IEEE Trans. Antennas Propag.*, vol. 61, no. 8, pp. 4275–4283, Aug. 2013.
- [22] I. Vasilev, V. Plicanic, and B. K. Lau, "Impact of antenna design on MIMO performance for compact terminals with adaptive impedance matching," *IEEE Trans. Antennas Propag.*, vol. 64, no. 4, pp. 1454–1465, 2016.
- [23] I. Vasilev and B. K. Lau, "On user effects in MIMO handset antennas designed using characteristic modes," *IEEE Antennas Wireless Propag. Lett.*, vol. 15, pp. 758–761, 2016.
- [24] J. Felício, J. Bioucas-Dias, J. Costa, and C. Fernandes, "Antenna design and near-field characterization for medical microwave imaging applications," *IEEE Trans. Antennas Propag.*, vol. 67, no. 7, pp. 2142–2153, 2019.
- [25] B. Xiao, H. Wong, B. Wang, and K. L. Yeung, "Effect of the screen to metal-frame smartphone antennas," in *Proc. IEEE Int. Workshop Antenna Technol. (iWAT)*, Miami, FL, Mar. 3–6, 2019, pp. 29–32.
- [26] B. Xiao, H. Wong, D. Wu, and K. L. Yeung, "Metal-frame antenna for big-screen smartphones using characteristic mode analysis," *IEEE Access*, vol. 7, pp. 122224–122231, 2019.
- [27] H. Aliakbari, L. Nie, and B. K. Lau, "Large screen enabled tri-port MIMO handset antenna for low LTE bands," *TechRxiv*, Apr. 4, 2020.
- [28] "Specifications | Samsung Galaxy S9 and S9+," The Official Samsung Galaxy Site. [Online]. Available: <https://www.samsung.com/global/galaxy/galaxy-s9/specs/>.
- [29] J. Liu, Q. Xue, H. Wong, H. W. Lai, and Y. L. Long, "Design and analysis of a low-profile and broadband microstrip monopolar patch antenna," *IEEE Trans. Antennas Propag.*, vol. 61, no. 1, pp. 11–18, Jan. 2013.
- [30] R. Martens and D. Manteuffel, "Systematic design method of a mobile multiple antenna system using the theory of characteristic modes," *IET Microw. Antennas Propag.*, vol. 8, no. 12, pp. 887–893, Sep. 2014.
- [31] H. Aliakbari and B. K. Lau, "On modal excitation using capacitive coupling elements and matching network," in *Proc. IEEE Int. Symp. Antennas Propag. (APS'2019)*, Atlanta, GA, Jul. 7–12, 2019.
- [32] J. Choi, W. Hwang, C. You, B. Jung, and W. Hong, "Four-element reconfigurable coupled loop MIMO antenna featuring LTE full-band operation for metallic-rimmed smartphone," *IEEE Trans. Antennas Propag.*, vol. 67, no. 1, pp. 99–107, Jan. 2019.
- [33] N. Peitzmeier and D. Manteuffel, "Systematic design of an ultra-wideband six-port multi-mode antenna element using symmetry properties of characteristic modes," in *Proc. IEEE Int. Conf. Electromagn. Adv. Appl. (ICEAA)*, Granada, Spain, Sep. 9–13, 2019, pp. 466–471.
- [34] T. Y. Shih and N. Behdad, "Bandwidth enhancement of platform-mounted HF antennas using the characteristic mode theory," *IEEE Trans. Antennas Propag.*, vol. 64, no. 7, pp. 2648–2659, 2016.
- [35] H. Aliakbari, M. Mosalanejad, C. Soens, G. A. E. Vandenbosch, and B. K. Lau, "Wideband SIW-based low-cost multilayer slot antenna array for E-band applications," *IEEE Trans. Compon., Packag., Manuf., Technol.*, vol. 9, no. 8, pp. 1568–1575, Aug. 2019.
- [36] J. Villanen, J. Ollikainen, O. Kivekäs, and P. Vainikainen, "Coupling element based mobile terminal antenna structures," *IEEE Trans. Antennas Propag.*, vol. 54, no. 7, pp. 2142–2153, 2006.